Electronic Supplementary Material (ESI) for Sustainable Energy & Fuels.

Supporting information

Bubble-Induced Convection Stabilizes Local pH during Solar Water Splitting in Neutral pH Electrolytes

Keisuke Obata,[a] and Fatwa F. Abdi,*[a]*

[a] Institute for Solar Fuels, Helmholtz-Zentrum Berlin für Materialien und Energie GmbH, Hahn-Meitner-Platz 1, 14109 Berlin, Germany

Correspondence and requests for materials should be addressed to Keisuke Obata (email: keisuke.obata@helmholtz-berlin.de) and Fatwa F. Abdi (email: fatwa.abdi@helmholtz-berlin.de)

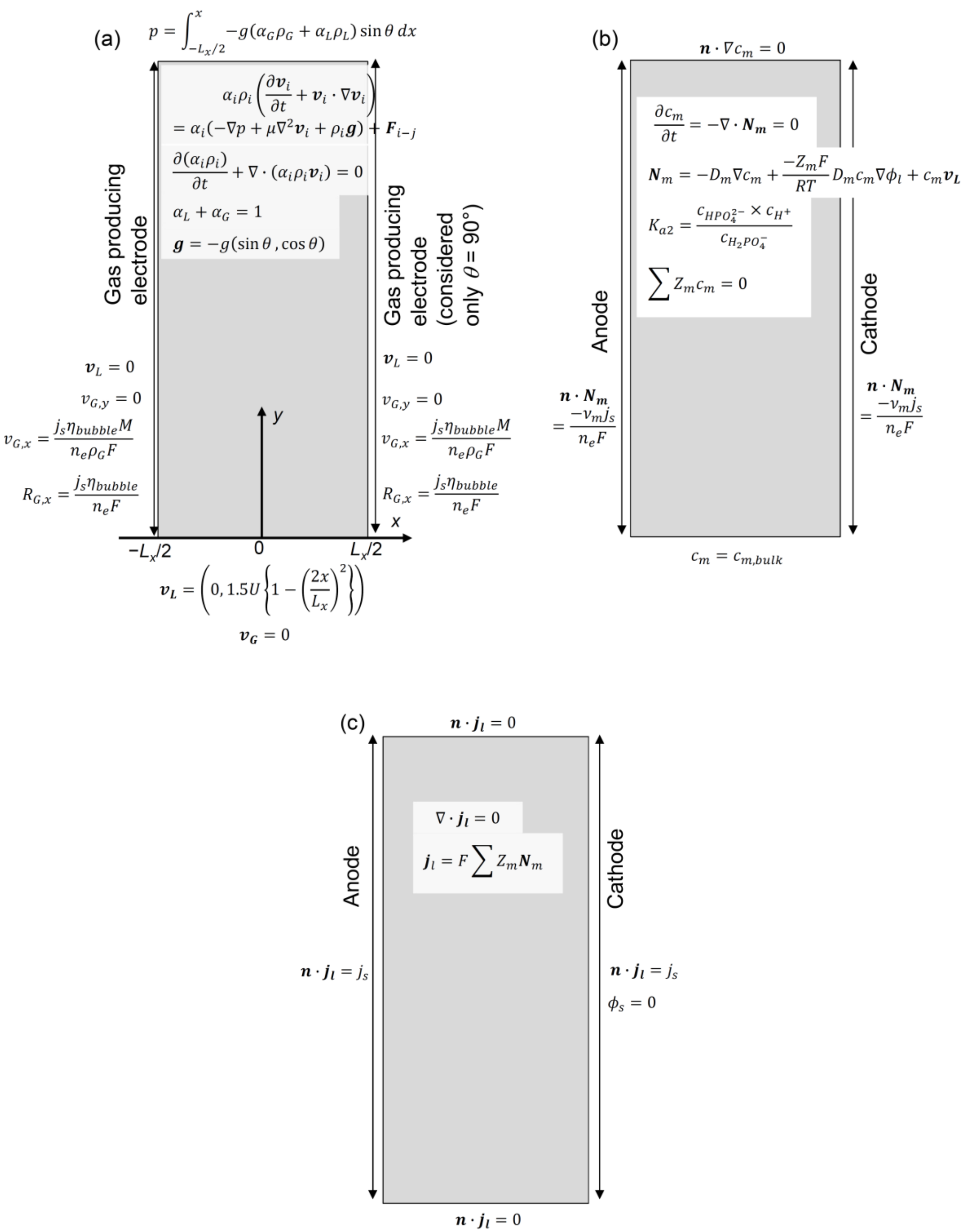

Figure S1. Schematic descriptions of our multiphysics model, showing the equations and boundary conditions for **(a)** multiphase fluid dynamics, **(b)** mass-transport, and **(c)** electrochemistry.

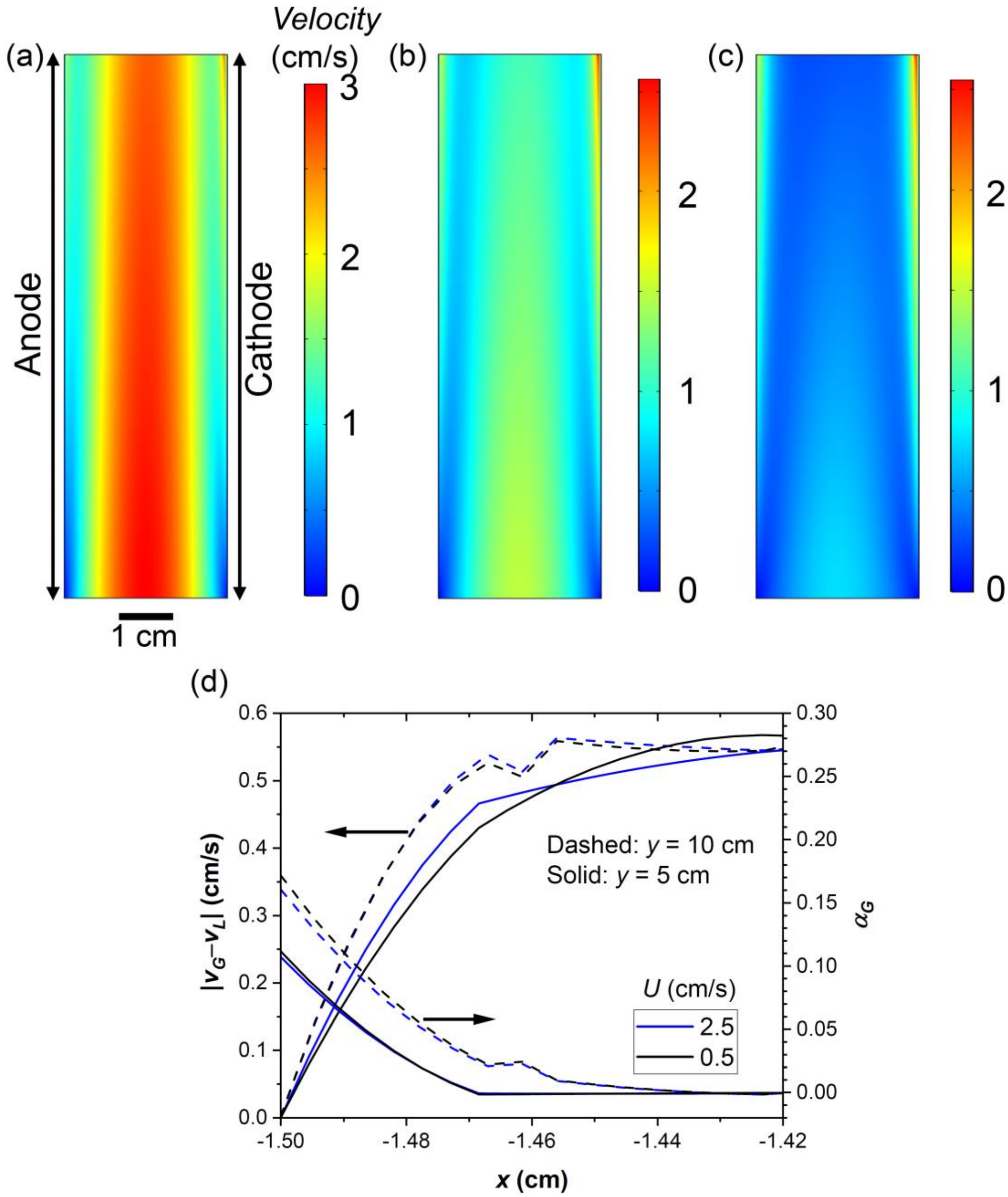

Figure S2. Velocity colormaps of the liquid phase in the 2-D channel with vertically oriented electrodes for the average inlet velocity, U = (a) 2, (b) 1, and (c) 0.5 cm/s. (d) Profiles of the gas volume fraction (α_G) and the relative velocity between the liquid and gas phase ($|v_G - v_L|$) for different U and at various y-position along the electrode. The average current density is 10 mA/cm^2, the bubble diameter is 0.1 mm, and the bubble formation efficiency is 0.5.

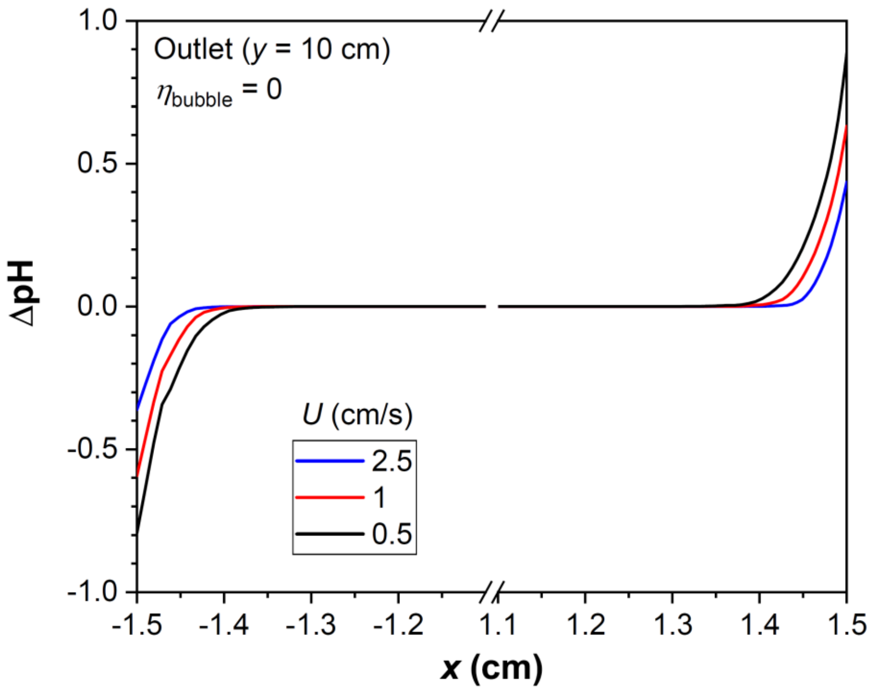

Figure S3. ΔpH profile from the anode to the cathode at the outlet simulated with the single-phase laminar flow (η_{bubble} = 0). The average current density is 10 mA/cm^2.

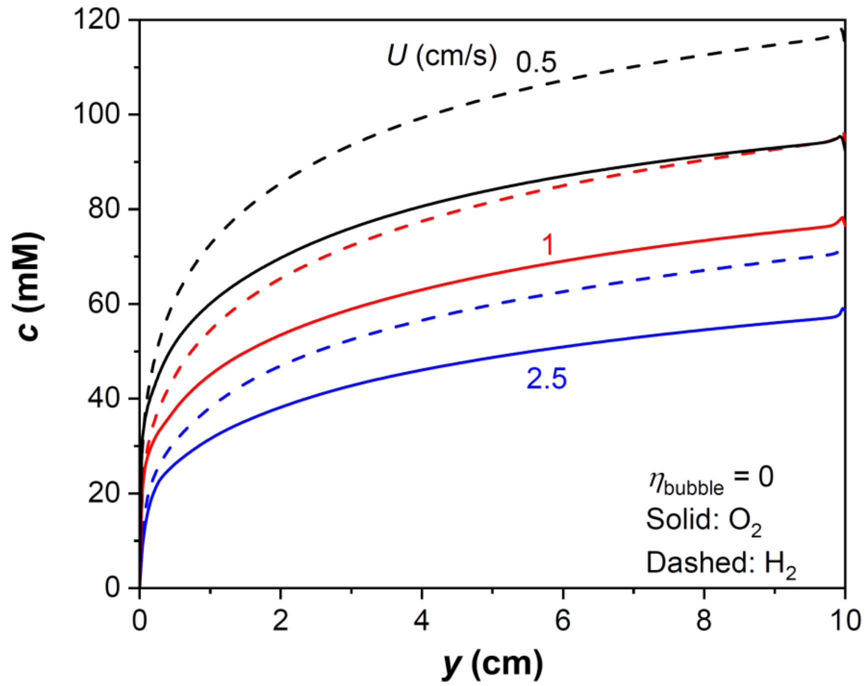

Figure S4. Concentration profile of the dissolved gases along the electrodes in the absence of gas bubbles. The average current density is 10 mA/cm^2.

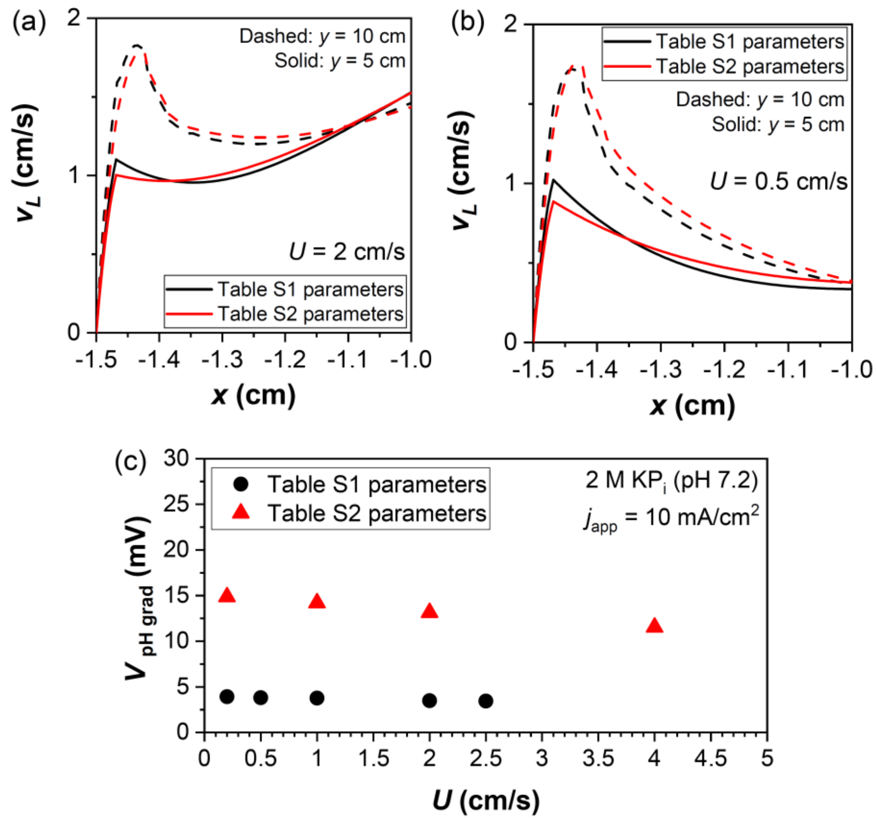

Figure S5. (a) – **(b)** Velocity profile of the liquid phase using the parameters shown in Table S1 and S2. U = **(a)** 2, and **(b)** 0.5 cm/s. **(c)** The resultant voltage losses due to the pH gradient. The average current density is 10 mA/cm^2, the bubble diameter is 0.1 mm, the bubble formation efficiency is 0.5, and $\theta = 90°$.

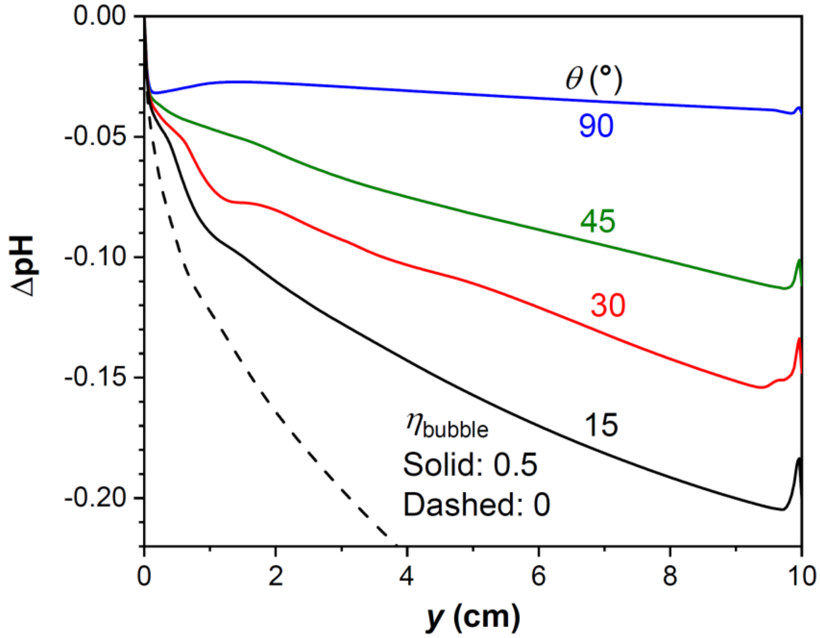

Figure S6. The resultant ΔpH along the upward-facing anode at different tilt angle, θ. The average current density is 10 mA/cm^2, the inlet velocity is 2.5 cm/s, the bubble formation efficiency is 0.5, and the bubble diameter is 0.1 mm. Sacrificial cathodic reaction is introduced to avoid the complete depletion of proton on the downward-facing electrode.

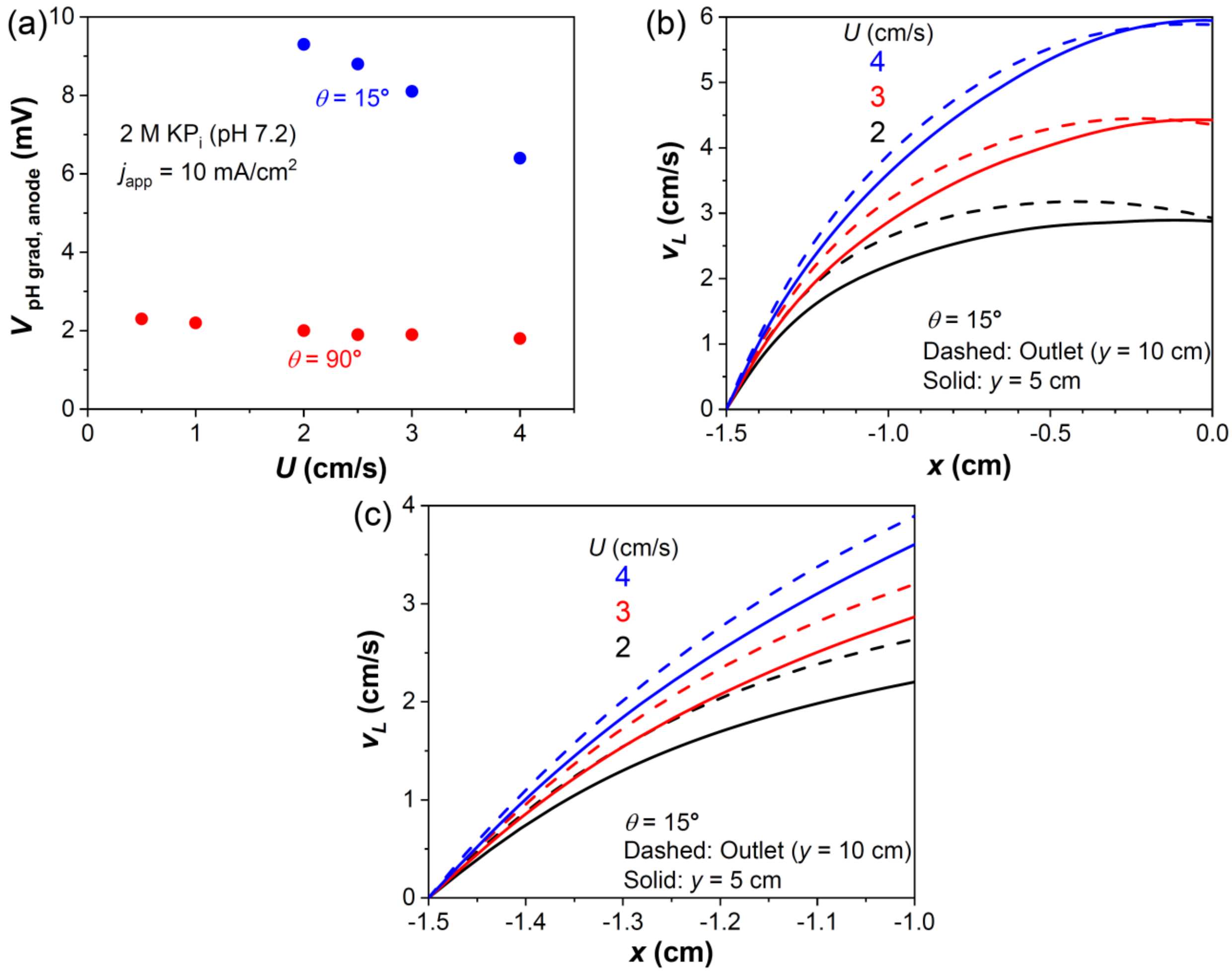

Figure S7. (a) Voltage loss due to pH gradient on the anode with different average inlet velocities at θ = 15 and 90°. **(b)** Velocity profile of the liquid phase close to the anode at θ = 15°. **(c)** Magnification of profiles shown in (b) at 5 mm away from the anode. The average current density is 10 mA/cm^2, the bubble formation efficiency is 0.5 and the bubble diameter 0.1 mm. Sacrificial cathodic reaction is introduced to avoid the complete depletion of proton on the downward-facing electrode.

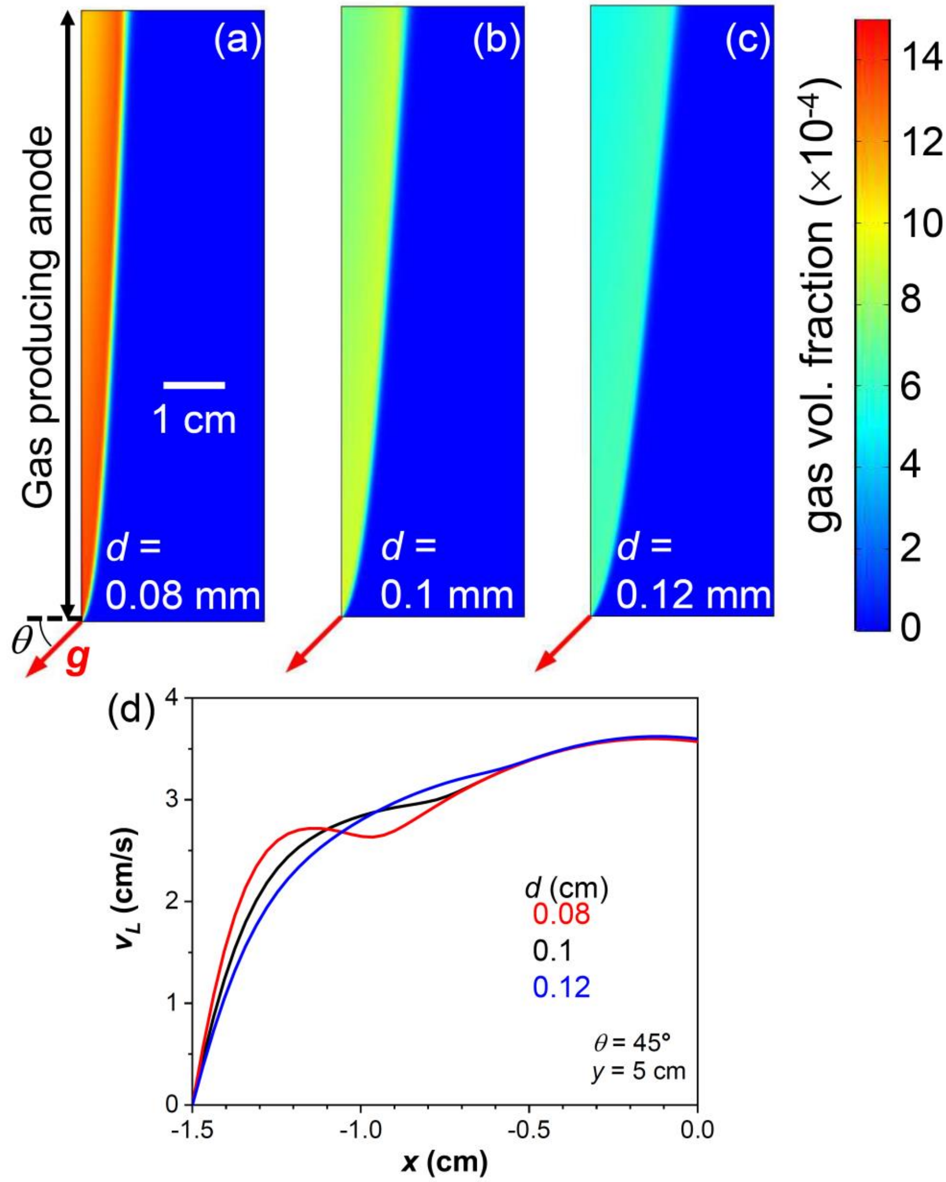

Figure S8. **(a)** – **(c)** Volume fraction colormaps of O_2 bubbles for various bubble diameters, *d* of **(a)** 0.08, **(b)** 0.1, and **(c)** 0.12 mm. **(d)** The respective velocity profile in the 2-D channel. The average current density is 10 mA/cm^2, the inlet velocity is 2.5 cm/s, the bubble formation efficiency is 0.5, and $\theta = 45°$.

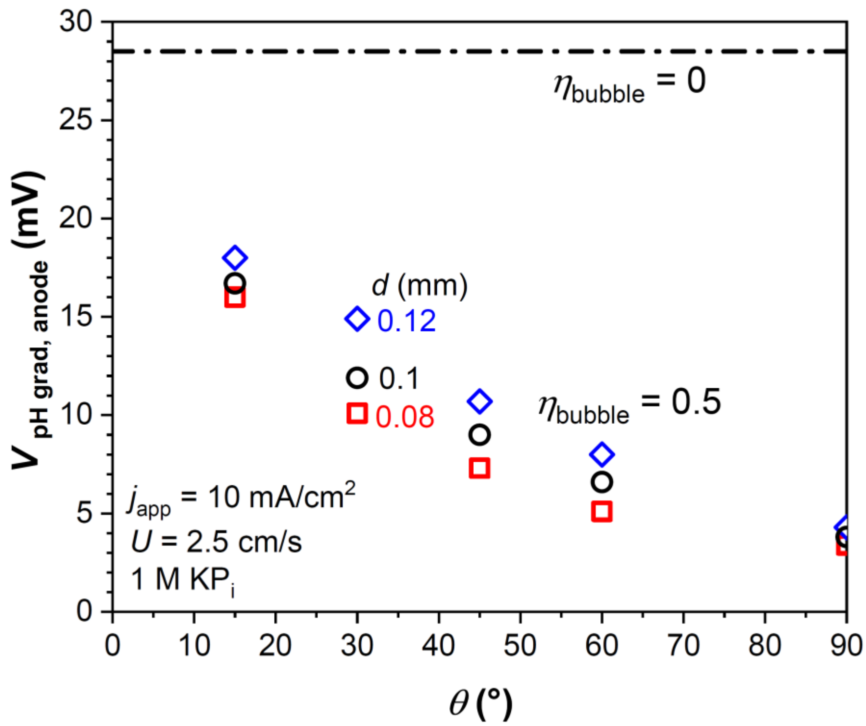

Figure S9. Voltage loss due to pH gradient on the anode with different device tilt angles, θ, and bubble diameters, d, in 1 M KP_i. The average current density is 10 mA/cm^2, the average inlet velocity is 2.5 cm/s, the bubble diameter is 0.1 mm, and the bubble formation efficiency is 0.5. For comparison, the horizontal dashed-dot line shows the same voltage loss in the absence of bubble-induced convection ($\eta_{bubble} = 0$).

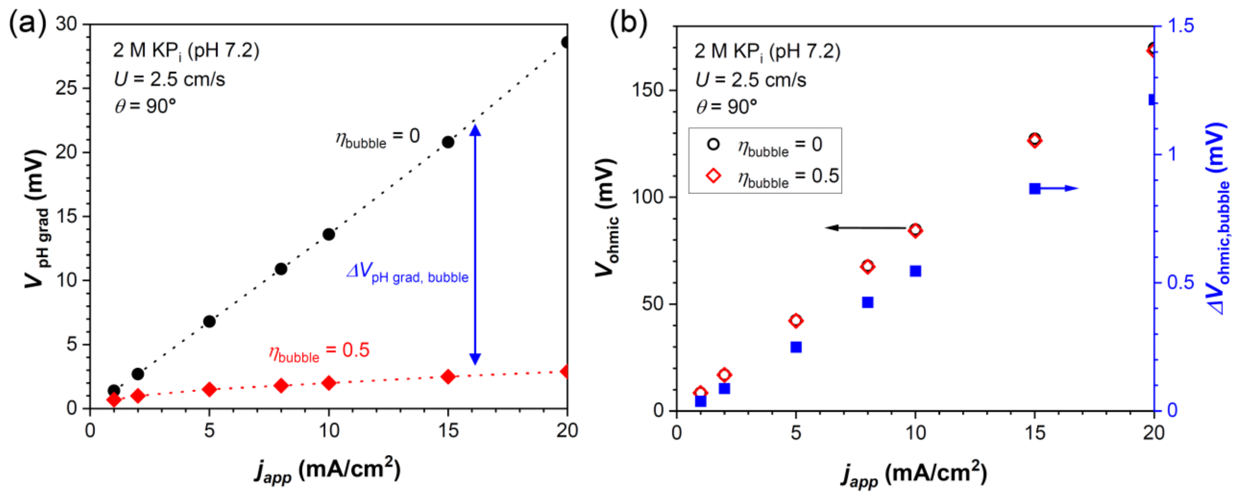

Figure S10. (a) Voltage loss due to the pH gradient on the anode at different current densities in 2 M KP$_i$. **(b)** Comparison of ohmic voltage losses in the electrolyte. The average current density is 10 mA/cm^2, the inlet velocity is 2.5 cm/s, the bubble diameter is 0.1 mm, the bubble formation efficiency is 0.5, and θ = 90°.

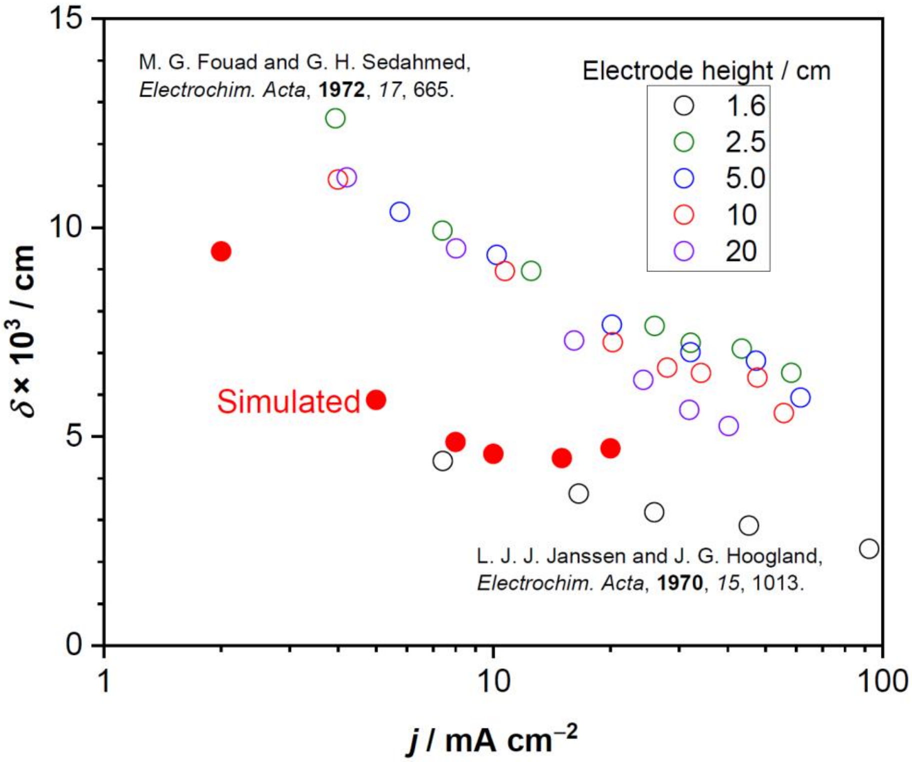

Figure S11. The effective diffusion layer thickness as a function of current density in the presence of gas bubbles, which was estimated according to methods shown in Supplemental note S1. The estimated thicknesses (red solid circles) are compared with those obtained experimentally on vertical electrodes during oxygen evolution reaction in previous reports.[1,2]

Table S1. Parameters used for our multiphysics simulations.

Parameters	Value	Ref.
Diffusion coefficient of dissolved H_2, D_{H_2}	5.0×10^{-9} [m^2/s]	3
Diffusion coefficient of dissolved O_2, D_{O_2}	2.4×10^{-9} [m^2/s]	3
Diffusion coefficient of H^+, D_{H^+}	9.3×10^{-9} [m^2/s]	3
Diffusion coefficient of K^+, D_{K^+}	1.96×10^{-9} [m^2/s]	3
Diffusion coefficient of $H_2PO_4^-$, $D_{H_2PO_4^-}$	0.85×10^{-9} [m^2/s]	3
Diffusion coefficient of HPO_4^{2-}, $D_{HPO_4^{2-}}$	0.69×10^{-9} [m^2/s]	3
Bulk concentration of dissolved H_2, $c_{H_2,bulk}$	0 [mol/L]	
Bulk concentration of dissolved O_2, $c_{O_2,bulk}$	0 [mol/L]	
Bulk concentration of H^+, $c_{H^+,bulk}$	$1.0 \times 10^{-7.21}$ [mol/L]	
Bulk concentration of K^+, $c_{K^+,bulk}$	1 [mol/L]	
Bulk concentration of $H_2PO_4^-$, $c_{H_2PO_4^-,bulk}$	1 [mol/L]	
Bulk concentration of HPO_4^{2-}, $c_{H_2PO_4^{2-},bulk}$	1 [mol/L]	
2nd buffer equilibrium constant, K_{a2}	$1.0 \times 10^{-7.21}$ [mol/L]	3
Dynamic viscosity of liquid, μ_L	8.9×10^{-4} [Pa s]	3
Density of liquid, ρ_L	0.997 [g/cm^3]	3
Density of gases, ρ_G	$3.2\times10^{-5}\times p/RT$ [g/cm^3]	
Molecular mass of gases, M	32 [g/mol]	
Gravitational acceleration, g	981 [cm/s^2]	
Temperature, T	298 [K]	

Parameter for electrochemistry	Value	Ref.
Exchange current density for OER, $j_{0,OER}$	1×10^{-5} mA/cm^2	4–7
Exchange current density for HER, $j_{0,HER}$	1 mA/cm^2	4,8
HER anodic transfer coefficient, $\alpha_{a,HER}$	0.5	
HER cathodic transfer coefficient, $\alpha_{c,HER}$	0.5	
OER anodic transfer coefficient, $\alpha_{a,OER}$	1.9	
OER cathodic transfer coefficient, $\alpha_{c,OER}$	0.1	

Table S2. Adjusted parameters used for the multiphysics simulations shown and compared in Figure S5.

Parameters	**Value**	**Ref.**
Diffusion coefficient of dissolved H_2, D_{H_2}	2.5×10^{-9} [m^2/s]	Estimated from 3 and μ_L using Stoke-Einstein equation
Diffusion coefficient of dissolved O_2, D_{O_2}	1.2×10^{-9} [m^2/s]	
Diffusion coefficient of H^+, D_{H^+}	4.7×10^{-9} [m^2/s]	
Diffusion coefficient of K^+, D_{K^+}	0.98×10^{-9} [m^2/s]	
Diffusion coefficient of $H_2PO_4^-$, $D_{H_2PO_4^-}$	0.43×10^{-9} [m^2/s]	
Diffusion coefficient of HPO_4^{2-}, $D_{HPO_4^{2-}}$	0.35×10^{-9} [m^2/s]	
Bulk concentration of dissolved H_2, $c_{H_2,bulk}$	0 [mol/L]	
Bulk concentration of dissolved O_2, $c_{O_2,bulk}$	0 [mol/L]	
Bulk activity of H^+, $c_{H^+,bulk}$	$1.0 \times 10^{-7.21}$ [mol/L]	
Bulk activity of K^+, $c_{K^+,bulk}$	0.6 [mol/L]	Estimated from 9,10
Bulk activity of $H_2PO_4^-$, $c_{H_2PO_4^-,bulk}$	0.3 [mol/L]	
Bulk activity of HPO_4^{2-}, $c_{H_2PO_4^{2-},bulk}$	0.3 [mol/L]	
2nd buffer equilibrium constant, K_{a2}	$1.0 \times 10^{-7.21}$ [mol/L]	3
Dynamic viscosity of liquid, μ_L	1.8×10^{-3} [Pa s]	Extrapolated from 11
Density of liquid, ρ_L	1.23 [g/cm^3]	Extrapolated from 3
Density of gases, ρ_G	$3.2 \times 10^{-5} \times p/RT$ [g/cm^3]	
Molecular mass of gases, M	32 [g/mol]	
Gravitational acceleration, g	981 [cm/s^2]	
Temperature, T	298 [K]	

Supplemental note S1: Evaluation of the effective diffusion layer thickness

The effective diffusion layer thickness in the presence of bubble-induced convection has been estimated by introducing a redox ion ($D_{red} = 3.5\times10^{-6}$ [cm^2/s], $c_{red} = 20$ [mM] at the inlet), similar to previous experimental reports.[1,2,12,13] The normal molar flux to the anode surface, N_{red}, was evaluated at the mass-transport limiting condition ($c_{red} = 0$ [mM] at the surface) in the velocity field obtained at various current densities during the study shown in Fig. 5. Due to the presence of supporting buffer ions, migration has been ignored. The effective diffusion layer thickness, δ, was obtained according to the Fick's first law shown below and plotted in Fig. S11.

$$\int_0^{L_y} N_{red} dy = \frac{D_{red} c_{red} L_y}{\delta} \qquad \text{(S1)}$$

References

1 L. J. J. Janssen and J. G. Hoogland, *Electrochim. Acta*, 1970, **15**, 1013–1023.

2 M. G. Fouad and G. H. Sedahmed, *Electrochim. Acta*, 1972, **17**, 665–672.

3 D. R. Lide, *Handbook of Chemistry and Physics*, CRC Press, Boca Raton, FL, 84th ed., 2003.

4 S. Haussener, C. Xiang, J. M. Spurgeon, S. Ardo, N. S. Lewis and A. Z. Weber, *Energy Environ. Sci.*, 2012, **5**, 9922–9935.

5 G. Lodi, E. Sivieri, A. De Battisti and S. Trasatti, *J. Appl. Electrochem.*, 1978, **8**, 135–143.

6 M. G. Walter, E. L. Warren, J. R. McKone, S. W. Boettcher, Q. Mi, E. A. Santori and N. S. Lewis, *Chem. Rev.*, 2010, **110**, 6446–6473.

7 K. Kinoshita, *Electrochemical oxygen technology*, John Wiley & Sons, Inc., 1992.

8 S. Trasatti, *J. Electroanal. Chem. Interfacial Electrochem.*, 1972, **39**, 163–184.

9 M. El Guendouzi and A. Benbiyi, *Fluid Phase Equilib.*, 2014, **369**, 68–85.

10 M. El Guendouzi and A. Benbiyi, *Fluid Phase Equilib.*, 2016, **408**, 223–231.

11 K. Obata, L. Stegenburga and K. Takanabe, *J. Phys. Chem. C*, 2019, **123**, 21554–21563.

12 L. J. J. Janssen and J. G. Hoogland, *Electrochim. Acta*, 1973, **18**, 543–550.

13 P. A. Kempler, R. H. Coridan, N. S. Lewis and N. S. Lewis, *Energy Environ. Sci.*, 2020, **13**, 1808–1817.